The Insertion of Nanoparticle Clusters into Vesicle Bilayers

Cécile Bonnaud[†,‡,], Christophe A. Monnier[†,*], Davide Demurtas[§], Corinne Jud[†], Dimitri Vanhecke[†], Xavier Montet[º], Ruud Hovius[″], Marco Lattuada[†], Barbara Rothen-Rutishauser[†,#], Alke Petri-Fink[†,‡]*

[†] Adolphe Merkle Institute, University of Fribourg, Route de l'Ancienne Papéterie CP209, 1723 Marly 1, Switzerland.

[‡] Chemistry Department, University of Fribourg, Chemin du Musée 9, 1700 Fribourg, Switzerland.

[§] Interdisciplinary Center for Electron Microscopy, Ecole Polytechnique Fédérale de Lausanne, Station 15, 1015 Lausanne, Switzerland.

[º] Radiology Department, Geneva University Hospital, Rue Gabrielle-Perret-Gentil 4, 1211 Genève 14, Switzerland.

[″] Laboratory of Physical Chemistry of Polymers and Membranes, Ecole Polytechnique Fédérale de Lausanne, Station 6, 1015 Lausanne, Switzerland.

[#] Respiratory Medicine, Bern University Hospital, Inselspital, Freiburgstrasse, 3010 Bern, Switzerland.

* These authors contributed equally to this work

Correspondence: alke.fink@unifr.ch

Supporting information

Liposomes and Their Reactions to Surfactant Exposure

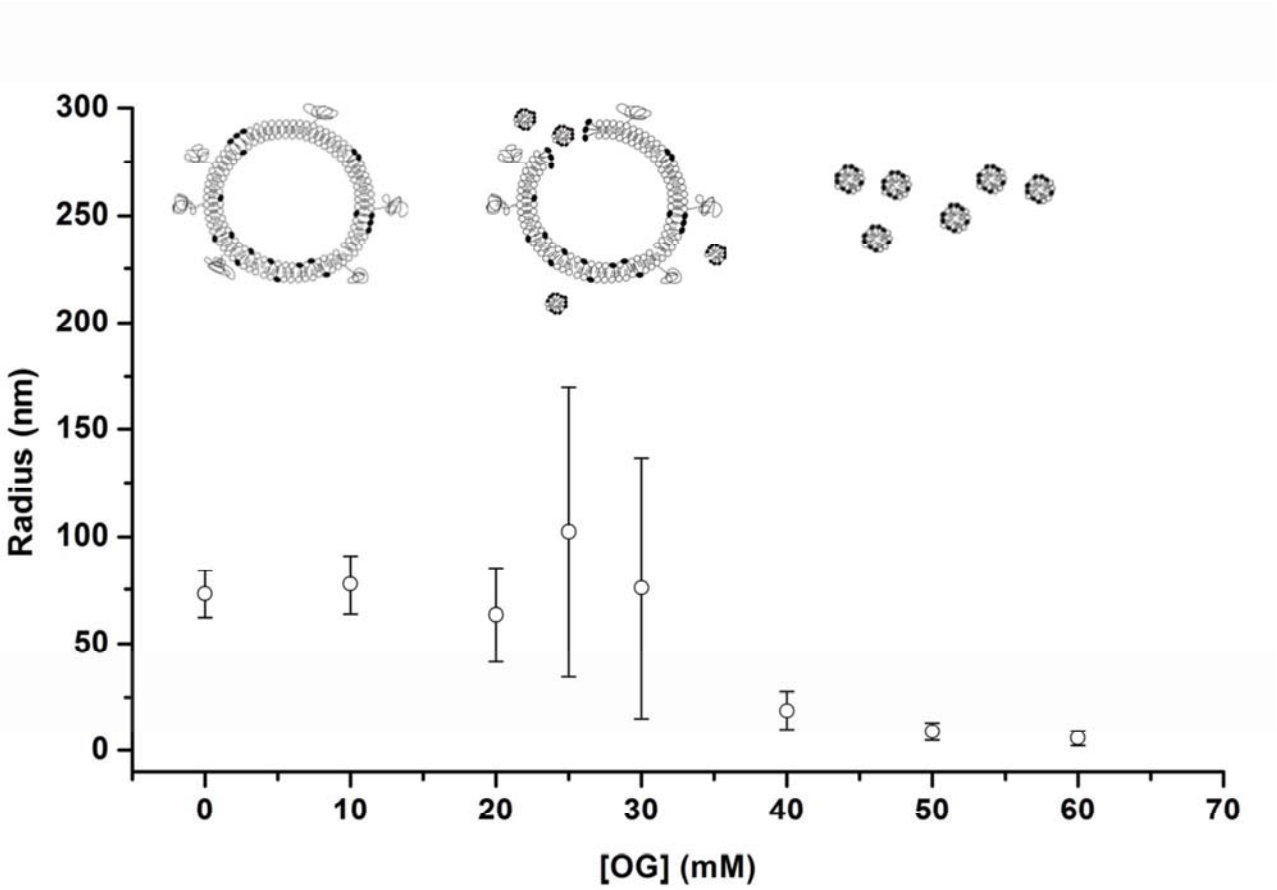

Suppl. Figure 1. Destabilization of pre-formed liposomes by surfactant addition (OG). Mean ± SD.

We additionally analyzed the liposome size distribution by dynamic light scattering (DLS) as a function of increasing OG concentration. Liposome stability began to decrease when a concentration around 25 mM is reached, which corresponds to the overall critical micelle concentration (25-30 mM) of octyl glucoside (OG). As soon as the surfactant CMC was reached, the lipid bilayer begins to undergo a transition from an organized structure to individual micelles. Above this concentration, a complete solubilization resulting in micelles composed of phospholipids and surfactant could be observed.

Cryo-TEM – Stage Tilting and Tomographic Cluster Analysis

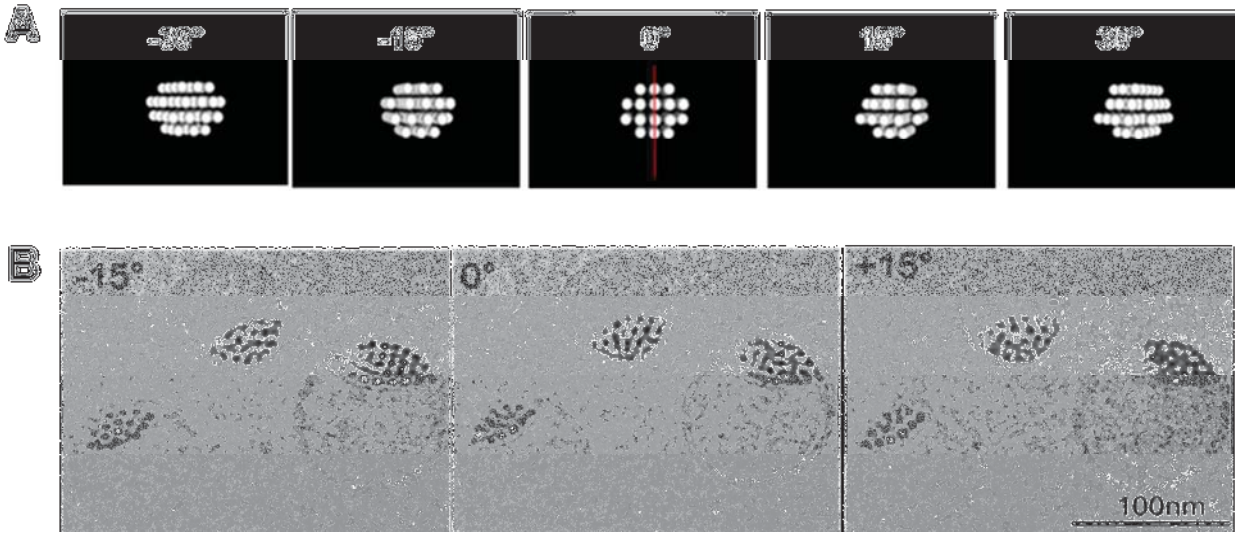

Suppl. Figure 2. Two-dimensional projections of densely packed nanoparticle clusters. Clusters composed of spherical nanoparticles which are packed layer-by-layer (A) exhibit different projection patterns at different angles. These differences can be highlighted by cryo-TEM stage tilting (B).

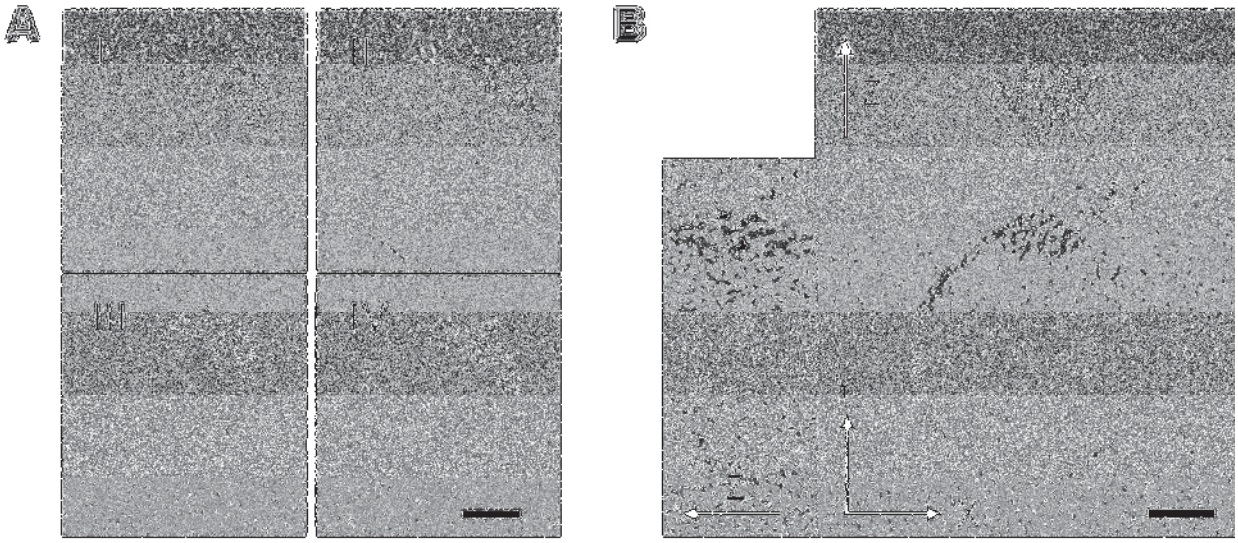

Suppl. Figure 3. Cryo-EM tomography for three-dimensional characterization of Janus magnetic liposomes and their incorporated clusters. Tomographic reconstruction from recorded tilt series enabled the investigation of individual slices at various Z-heights within the specimen (A, I-IV). This information revealed the dense and hexagonally organized packing of the nanoparticles within the cluster (Suppl. movie). Scale bars = 50 nm

Janus Magnetic Liposome Re-Assembly – Dynamic Light Scattering and Overall Homogeneity

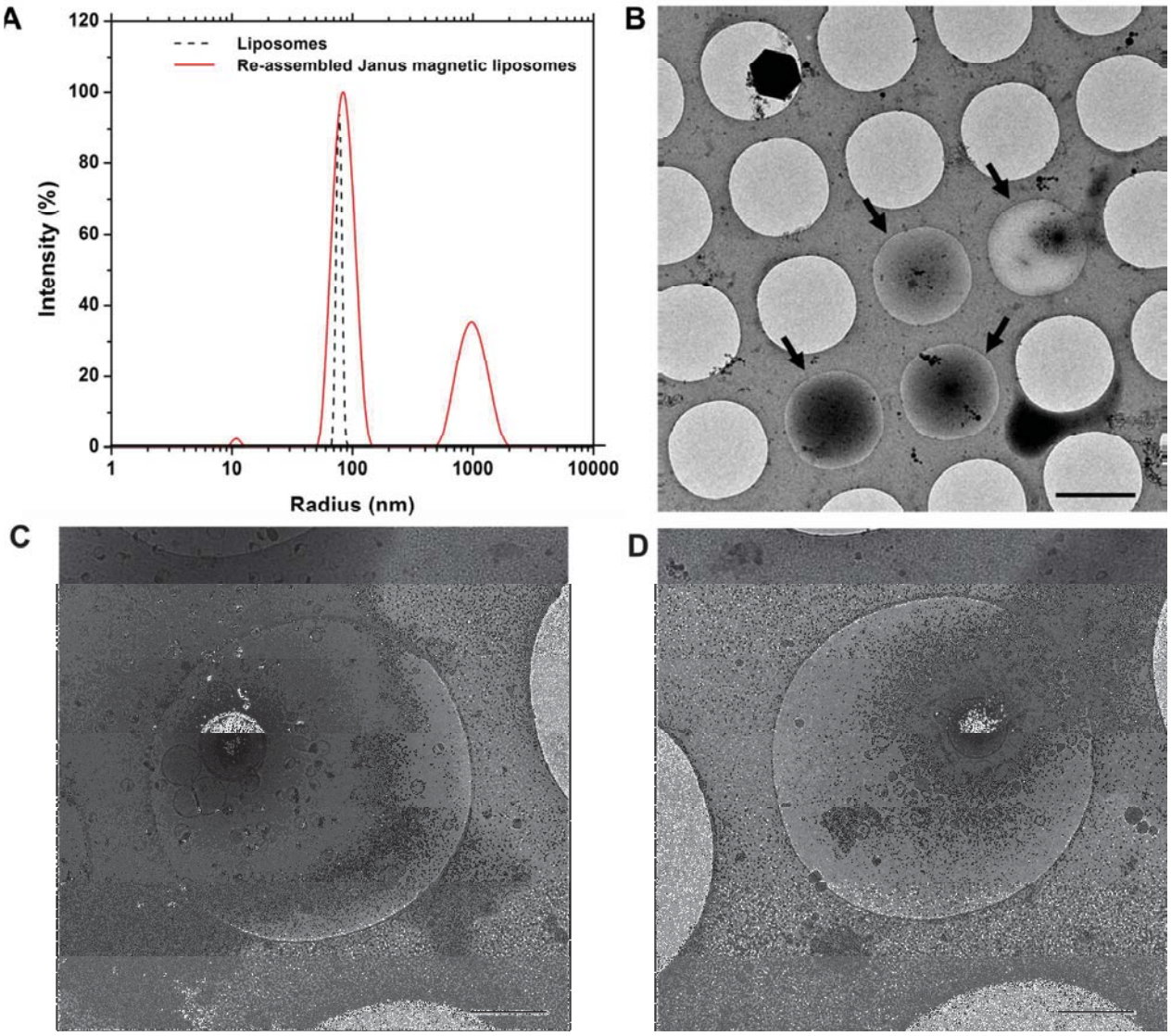

Suppl. Figure 4. Liposome size analysis by DLS before and after re-assembly. Pre-formed liposomes were compared to their reassembled counterparts containing nanoparticle clusters (A). These measurements were then correlated to low-magnification cryo-TEM images (B-D). Within the overall grid, areas with vitreous ice are clearly visible (A, scale bar = 2000 nm). At a higher magnification, the vesicles become distinguishable from each other (C/D, scale bar = 500 nm). Cluster-liposome hybrids can be identified due to the darker contrast of the clusters and their morphology. From these overviews, a general impression on sample distribution and homogeneity can be drawn.

Membrane Energetics – Additional Considerations

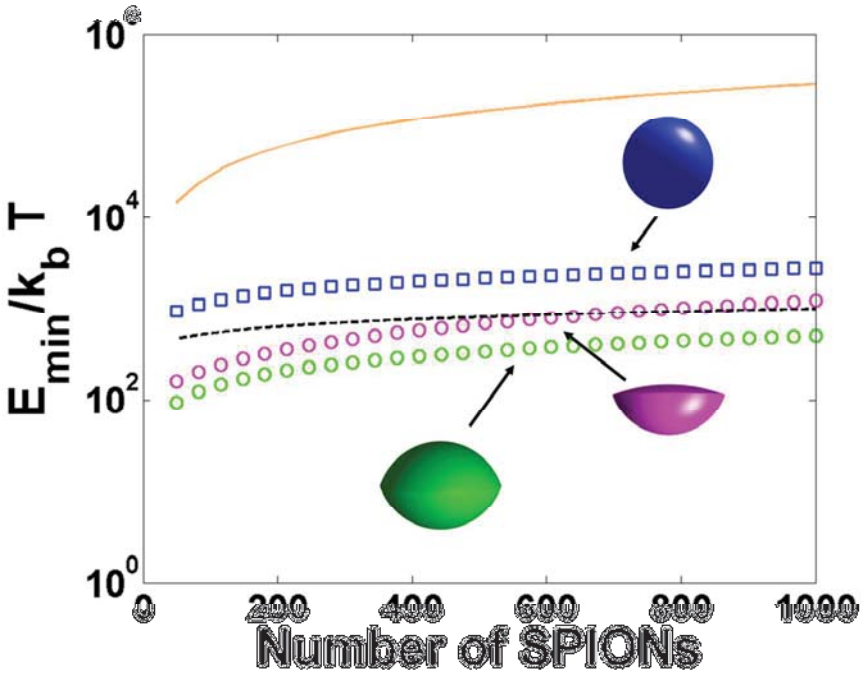

Suppl. Figure 5. The energy of different inclusions, including isolated spherical clusters and single nanoparticles. The inclusion energy of an asymmetric spherical cap geometry, having a radius equal to the liposome radius (taken equal to 50 nm), was plotted as a function of the number of nanoparticles within the inclusion. The energy of a corresponding spherical inclusion is additionally shown for comparison (blue), along with that of a spherical cluster covered by a lipid monolayer (black dashed line). The energy of an equal number of nanoparticles each individually covered by a lipid monolayer is represented by the continuous orange line.

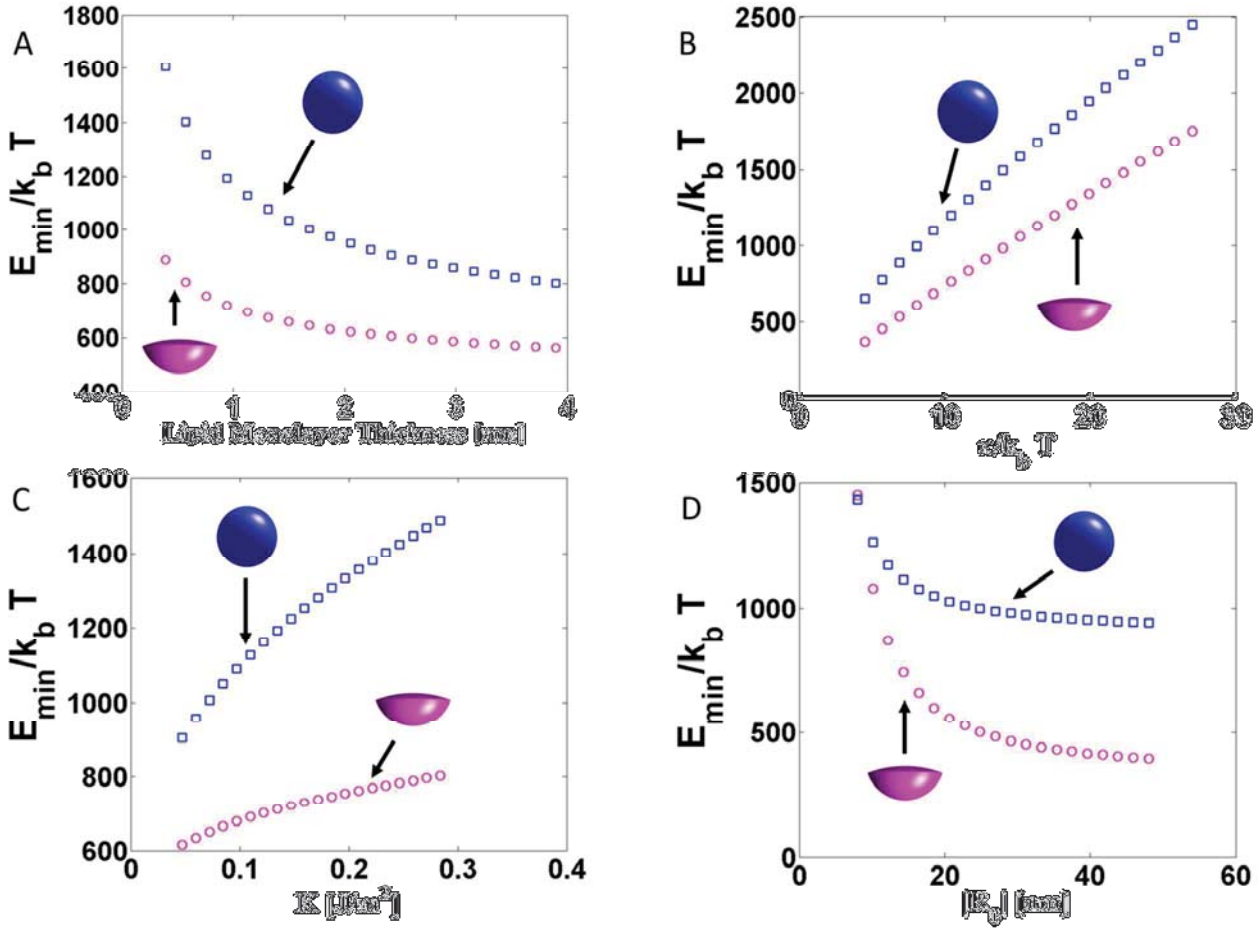

Suppl. Figure 6. The inclusion energy dependence on physical parameter values. The inclusion energy of an symmetric spherical cap geometry, having a radius equal to the liposome radius (taken equal to 50 nm), has been compared to that of a spherical inclusion. Both inclusions are composed of 500 nanoparticles and plotted as a function of alkyl chain length (A), bending modulus (B), stretching modulus (C) and bilayer spontaneous curvature radius (D). As the alkyl chain length increases, the inclusions energy decreases, as the stretching contribution is inversely proportional to the chain length. As the bending of stretching moduli increase, the inclusion energy increases, being the energy proportional to the moduli. The inclusion energy also increases as the spontaneous curvature radius decreases in absolute value. In all cases, the inclusion energy changes in a similar fashion for both types of inclusions.

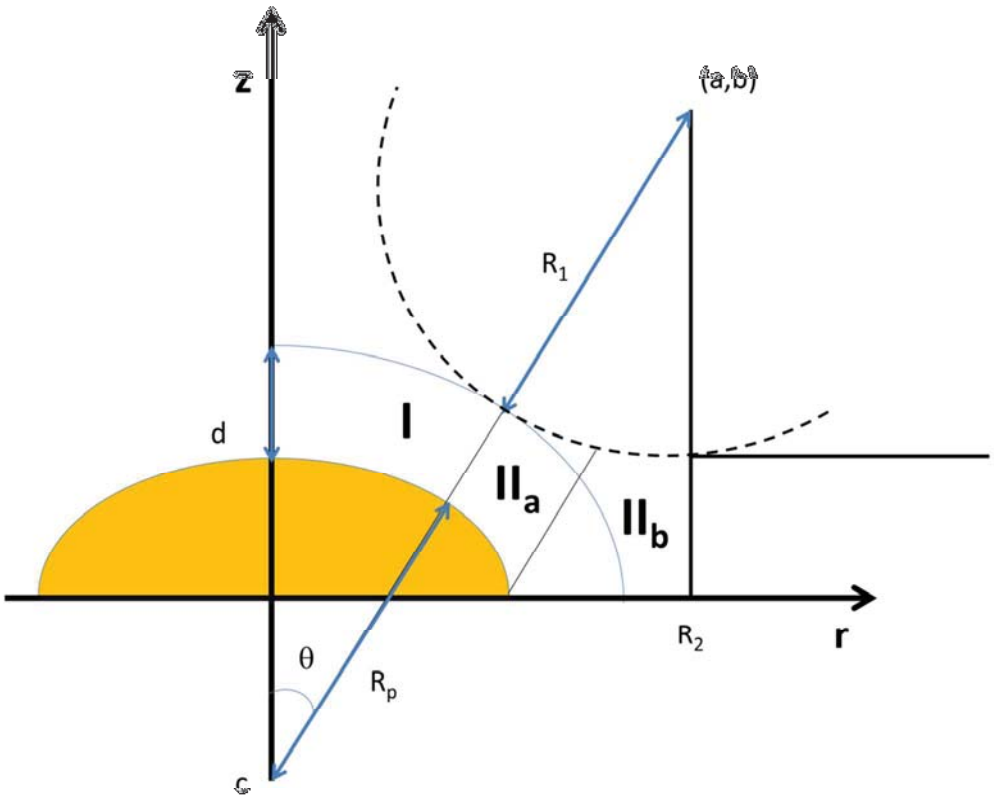

Suppl. Figure 7. Schematic of the inclusion geometry assuming a spherical cap shape. In region *I*, the hydrocarbon chains keep their lipid monolayer thickness *d* without any stretching or compression. The local curvature radius is equal to $R_p + d$. In region II, the chains are stretched from *d*.

SAXS - Curve fitting

The scattered intensity I(q) of the samples was recorded as a function of the scattering vector q:

$$q = \left(\frac{4\pi}{\lambda}\right) \times \sin\left(\frac{\theta}{2}\right) \quad (1.1)$$

λ is the wavelength and θ the scattering angle. From the scattering curve, information is obtained on both the shape of a single object and the structure of several objects (i.e. their correlation in space). At low concentrations, no structure is detected and only information about the shape is obtained. A scattering curve obtained from such a diluted sample is an effective form factor Peff(q).

For oleic acid-coated SPIONs, the best curve fitting, obtained using a sphere model (Equations 2 and 3):

$$I_{sphere}\,(Q,R) = K^2(Q,R,\Delta\eta) \quad (1.2)$$

$$K(Q,R,\Delta\eta) = \frac{4}{3}\pi R^3 \Delta\eta^3 \frac{\sin(QR) - QR\cos(QR)}{(QR)^3} \quad (1.3)$$

I is the scattering intensity for the sphere in function of the scattering vector q. The sphere radius R and the scattering length density difference between the particle and the solvent Δη. The nanoparticle distribution follows a log normal distribution and is continuous in which the logarithm of a variable X has a normal distribution. Therefore, the model includes Equations 4 and 5:

$$LogNorm(X,\mu,p,\sigma) = \frac{N}{CLN\ X^p} \exp\left(-\frac{ln\frac{X}{\mu}}{2\sigma^2}\right) \quad (1.4)$$

$$CLN = \sqrt{2\pi}\sigma\mu^{1-p} \exp\left((1-p)^2 \frac{\sigma^2}{2}\right) \quad (1.5)$$

μ is the location of the center or radius, σ the width of the distribution, p the shape of the distribution and N the number of particles. The fitting of the curve at high Q was obtained by adding a second contribution of a spherical model (μ = 1.5 □$^{-1}$, σ = 0.11, p = 0.1), which could be due to roughness of the surface from to oleic acid coating or porosity of the metal oxide. In our case however, this curve shape is probably an artifact caused by the reduction of the solvent form factor.